Available online at www.sciencedirect.com
ScienceDirect
Acta Materialia 55 (2007) 2173–2182
Acta MATERIALIA
www.actamat-journals.com

Pinning effect of second-phase particles on grain growth in polycrystalline films studied by 3-D phase field simulations

N. Moelans *, B. Blanpain, P. Wollants

Department of Metallurgy and Materials Engineering, Katholieke Universiteit Leuven, Kasteelpark Arenberg 44, B-3001 Leuven, Belgium

Received 16 June 2006; received in revised form 3 August 2006; accepted 9 November 2006
Available online 19 January 2007

Abstract

Three-dimensional simulations of grain growth in thin films containing finely dispersed second-phase particles were performed using a phase field model. The simulations show that although the growth behavior of the columnar grain structures in thin films is essentially two-dimensional, the interaction between the particles and the grain boundaries is three-dimensional. Grain boundaries can therefore more easily break free from the particles than in purely two-dimensional systems, resulting in fewer grain boundary–particle intersections and a larger final grain size. For a given volume fraction f_V and size of the particles r, the final grain size $\overline{R}_{lim}$ increases with film thickness. Moreover, it was found that particles located in the middle of the film are most efficient in pinning grain boundaries. A classical Zener type relation $\overline{R}_{lim}/r = K(1/f_V^b)$ cannot describe these effects.

Keywords: Phase field models; Simulation; Grain growth; Thin films; Zener pinning

1. Introduction

Grain growth in thin films is different from grain growth in bulk materials [1,2]. Once the grain size becomes larger than the thickness of the film, grains grow columnar, with their boundaries perpendicular to the plane of the film. Grain growth is then essentially two-dimensional (2-D), as grain boundaries are only significantly curved within the plane of the film. Yet three-dimensional (3-D) phenomena can considerably affect the growth behavior. The drag effect of thermal grooving at the film surface and the influence of additional driving forces, such as the orientation dependence of the surface energy or the film–substrate interfacial energy, or the strain energy, have been discussed several times [1–6]. In this article, it is shown that second-phase particles also introduce a 3-D effect in the migration of the columnar grain boundaries.

Small particles or impurities that lead to the formation of small precipitates are often added to thin films for extra pinning of the grain boundaries. Mostly, the purpose is to promote abnormal grain growth. The particles hinder normal grain growth so that a few grains, e.g. those with a low surface energy, can grow abnormally at the expense of the other pinned matrix grains. In this way, films with large columnar grains that are many times (up to 1000) the thickness of the film are obtained [1,7–9]. Such films are wanted in micro-electronic applications since a large grain size reduces the rate of failure due to electromigration.

Most analytical theories [10,11] for Zener pinning predict that normal grain growth is inhibited when a critical mean grain radius $\overline{R}_{lim}$ equal to

$$\frac{\overline{R}_{lim}}{r} = K\frac{1}{f_V^b} \tag{1}$$

is reached, where r is the particle radius and f_V the volume fraction of the second-phase particles. The value of the parameters K and b varies among the different theories. If the size and shape of a particle and the surface tensions associated with the grain boundaries and the particle matrix interface are known, the pinning force of the particles can be analytically calculated as a function of the position

* Corresponding author.
E-mail address: nele.moelans@mtm.kuleuven.be (N. Moelans).

1359-6454/$30.00
doi:10.1016/j.actamat.2006.11.018

of the grain boundary [10–14]. The calculation of the total pinning force of a dispersion of particles on a unit area of grain boundary, on the other hand, is more complex. Not all the particles lie on a grain boundary and it appears to be extremely difficult to determine the fraction ϕ of particles that effectively contributes to the pinning effect. Moreover, the pinning force exerted at each grain boundary–particle intersection depends on the geometry of the grain boundary near the grain boundary–particle intersection. All analytical theories make approximations in calculating the pinning force of a dispersion of particles on a grain boundary network.

The pinning effect of second-phase particles is frequently studied by means of computer simulations based on Monte Carlo Potts [15–19], front-tracking (or vertex) [20–22], phase-field [23–26] and finite element models [27]. The main advantage of these techniques is that the whole microstructure, namely the shape and position of the grain boundaries is calculated as a function of time. As a consequence, no assumptions on the fraction of particles that is in contact with a grain boundary and the grain boundary profile at an intersection are required. Furthermore, compared with experimental studies, material and process parameters can be varied relatively easily and independently in computer simulations. A serious drawback is that simulations for grain growth require massive computer resources, especially in the case of 3-D simulations. For 2-D systems [15,17,18,20,21,23,25], the simulations show that most particles are in contact with a grain boundary ($\phi \approx 1$) and the final mean grain radius $\overline{R}_{\lim}$ obeys a relation of the form Eq. (1) with $b = 0.5$ and K between 1.2 and 1.7. For 3-D systems [16,19,24,26,27], it is clear that the fraction of particles in contact with a grain boundary ϕ is lower than in 2-D systems, but there is no agreement yet on the parameter values in relation (1).

Grain growth in thin films is usually treated with 2-D simulations [28,29]. Three-dimensional aspects, such as surface grooving [20,30], anisotropy in the surface energy of the grains [31] and substrate–film mismatches [32], are included as additional terms in the driving force for grain boundary migration. Also the pinning effect of second-phase particles in thin films was handled using a modified 2-D grain growth model [20]. However, in some respects, 2-D simulations do not agree with experimental findings for thin films. They predict, for example, that nearly all particles lie on grain boundaries [15,20,25], whereas in thin films there are many particles within the grains [9,33]. Two-dimensional simulations therefore overestimate the pinning effect of second-phase particles in thin films. Moreover, some experimental studies [7–9] revealed that particles located at or near the middle of the film are more effective. This feature might be interesting from an application point of view, yet it is completely ignored in 2-D simulations.

In this article, the pinning effect of second-phase particles on grain growth in thin films is studied from 3-D simulations based on a phase field model. The simulation results are compared with results from 2-D simulations and with experimental results obtained by Longworth and Thompson [9] for Al-alloy films containing Θ'-$CuAl_2$ precipitates.

2. Model, model parameters and numerical implementation

Phase field models for grain growth in the presence of second-phase particles were proposed by Fan et al. [23], Steinbach and Apel [24] and the present authors [34]. The latter model was applied to study the effect of second-phase particles on grain growth in 2-D systems [25] and 3-D [26] systems. The same model was used for the simulations discussed in this article. Much effort was made to reduce the computational requirements as far as possible. As a result, the model allows one to perform simulations for polycrystalline structures containing a large number of grains and particles and, at the same time, to resolve the shape of the grain boundaries near each particle–grain boundary intersection. A large number of grains and particles must be considered in the simulations to obtain statistically significant values for the final mean grain size. The evolution of the grain boundary profile near a grain boundary–particle intersection determines the distance over which the particle pins the grain boundary [13,35–37]. Therefore, the grain boundary shape near particle intersections must be treated explicitly in the simulations in order to predict the number of particles that is in contact with a grain boundary.

2.1. Model description

The model is based on the phase field model for normal grain growth in single phase materials of Chen [38] and Fan and Chen [39]. The different grains of the matrix phase are represented by a set of phase field variables

$$\eta_1(\mathbf{r},t), \eta_2(\mathbf{r},t), \ldots, \eta_p(\mathbf{r},t)$$

that are continuous functions of the spatial coordinates $\mathbf{r} = (x_1, x_2, x_3)$ and time t. A spatially varying function $\Phi(\mathbf{r})$ is used to describe the dispersion of second-phase particles. $\Phi(\mathbf{r})$ equals 1 within the particles and 0 outside the particles. It is assumed that the particle–matrix interface is incoherent and the particle dispersion is constant in time. The homogeneous free energy density of the system is formulated as a Landau polynomial of the phase field variables η_i

$$f_0(\eta_1,\eta_2,\ldots,\eta_p) = m\left(\sum_{i=1}^{p}\left(-\frac{\eta_i^2}{2}+\frac{\eta_i^4}{4}\right)+\sum_{i=1}^{p}\sum_{j\neq i}^{p}\eta_i^2\eta_j^2+\epsilon\Phi\sum_{i=1}^{p}\eta_i^2\right) \quad (2)$$

For $\Phi = 1$, the homogeneous free energy density has a single minimum at $(\eta_1, \eta_2, \ldots, \eta_p) = (0, 0, \ldots, 0)$. For $\Phi = 0$, the homogeneous free energy density has $2p$ minima with equal depth at

$$(\eta_1,\eta_2,\ldots,\eta_i,\ldots\eta_p) = (0,0,\ldots,\pm1,\ldots,0) \quad \text{for } i = 1\ldots p$$

distinguishing different matrix grains. It is assumed that $\eta_i = 1$ and $\eta_i = -1$ represent the same grain orientation. The temporal evolution of the η_is is described by Ginzburg–Landau equations

$$\frac{\partial \eta_i(\mathbf{r},t)}{\partial t} = -L\left[\frac{\partial f_0(\eta_1,\eta_2,\ldots)}{\partial \eta_i(\mathbf{r},t)} - \kappa\nabla^2\eta_i(\mathbf{r},t)\right] \tag{3}$$

with L a kinetic parameter and κ the gradient energy coefficient. A full description of the model was given in Ref. [34].

In this model, the pinning effect of the particles is based on the fact that when a particle and a grain boundary intersect, the total amount of grain boundary in the system is reduced by the intersection length (2-D) or area (3-D). Accordingly, new grain boundary area must be created before the grain boundary can break free from the particle. When a grain boundary meets a particle, the diffuse regions of the grain boundary and the particle–matrix interface overlap and interact. After a few time steps the original particle–matrix interface, corresponding to the equilibrium profile of the η_is is recovered. The grain boundaries neither go through the particles nor envelop them. This behavior conforms to the interaction mechanism assumed for most incoherent particles [10,11,13,14,40,41].

One problem of grain growth models derived from the model of Chen [38] is that when two neighboring grains are represented by the same phase field variable, they coalesce within a few time steps. A large number of phase field variables must be used to minimize the effect of this unphysical grain coalescence. According to Fan and Chen [39], 36 phase field variables suffice to obtain realistic grain growth behavior in 2-D systems. Later, Krill and Chen [42] showed that for more extensive grain growth and for 3-D grain growth much more phase field variables are required (up to 200 for 3-D simulations). Therefore, they developed a dynamic grain-orientation-reassignment technique that avoids grain coalescence and allows one to perform 3-D grain growth simulations for isotropic materials using far fewer phase field variables. Due to the pinning effect in the present simulations, the extent of grain growth and the frequency of grain coalescence were much smaller than in the simulations for normal grain growth of Krill and Chen. It was not necessary to check each time step whether grains represented by a same phase field variable were approaching each other, like in the dynamic grain-orientation-reassignment technique. Instead, after a certain amount of grain growth, all phase field variables were reassigned to the grains at the same time. Depending on the extent of grain growth, the reassignment procedure was performed 1–3 times during a simulation. A set of 30 phase field variables was used ($p = 30$). This approach does not completely exclude the coalescence of neighboring grains, though the frequency is largely reduced since phase field variables eliminated during extensive grain growth are reintroduced into the simulation. Moreover, phase field variables were assigned in such a way that grains represented by the same phase field variable were far from each other. Although the reassignment of phase field variables during a simulation does not correspond to a physical process, it is justifiable in the case of isotropic grain boundary properties since then all grain orientations are equivalent.

2.2. Numerical solution

A numerical method that combines a Fourier-spectral method [43] with a finite difference discretization was used to solve the phase field equations in 3-D for thin films. The Fourier-spectral method along with periodic boundary conditions was applied for the dimensions in the plane of the film. Due to the small thickness, periodic boundary conditions are not appropriate for the dimensions perpendicular to the plane of the film. Therefore, a finite difference discretization along with Dirichlet boundary conditions, namely $\eta_i = 0$, $\forall i$ at the top and the bottom of the film, was applied for the third dimension. A physical motivation for forcing the η_is to become 0 at the surface of the film is that the atomic ordering of the bulk material is distorted at surfaces.

The Fourier transform with respect to the coordinates x_1 and x_2 in the plane of the film of Eq. (3) gives

$$\begin{aligned}\frac{\partial \widetilde{\eta}(g_1,g_2,x_3,t)}{\partial t} = &-L\left(\widetilde{\frac{\partial f_0}{\partial \eta}}\right)(g_1,g_2,x_3,t)\\ &+L\kappa\left(-(g_1^2+g_2^2)\widetilde{\eta}(g_1,g_2,x_3,t)\right.\\ &\left.+\frac{\partial^2\widetilde{\eta}(g_1,g_2,x_3,t)}{\partial x_3^2}\right)\end{aligned} \tag{4}$$

where the subscript i is omitted to simplify the notation. g_1 and g_2 are coordinates in Fourier space related to x_1 and x_2 in real space. The functions $\widetilde{\eta}$ and $\widetilde{\frac{\partial f_0}{\partial \eta}}$ are, respectively, the Fourier transform of η and $\frac{\partial f_0}{\partial \eta}$. In practice, the Fourier transform is approximated by a discrete Fourier transform using a fast Fourier transform algorithm and the functions η and $\widetilde{\eta}$ are only defined in discrete points. The coordinates g_1 and g_2 take discrete values $n(2\pi/N\Delta x)$, with $n = -N/2+1, -N/2+2, \ldots, N/2$, Δx the grid spacing in real space and N the number of grid points in each dimension. For each point (g_1,g_2) in Fourier space, Eq. (4) is a partial differential equation in the spatial coordinate x_3 and time t. The equations are further discretized with respect to time and the spatial coordinate x_3 using a semi-implicit finite difference scheme, resulting in a set of coupled algebraic equations with unknowns $\widetilde{\eta}_s^{n+1}$

$$\begin{aligned}&-\left(\frac{L\kappa\Delta t}{(\Delta x)^2}\right)\widetilde{\eta}_{s-1}^{n+1} + \left(1 + L\kappa\Delta t(g_1^2+g_2^2) + 2\frac{L\kappa\Delta t}{(\Delta x)^2}\right)\widetilde{\eta}_s^{n+1}\\ &-\left(\frac{L\kappa\Delta t}{(\Delta x)^2}\right)\widetilde{\eta}_{s+1}^{n+1} = \widetilde{\eta}_s^{n} - L\Delta t\left(\widetilde{\frac{\partial f_0}{\partial \eta}}\right)_s^n.\end{aligned} \tag{5}$$

The index n refers to time steps and s to the discrete values of the x_3-coordinate. An inverse discrete Fourier transform of $\widetilde{\eta}_s^{n+1}(g_1,g_2)$ then gives $\eta_s^{n+1}(x_1,x_2)$. In the current work a con-

jugate gradient technique without preconditioner was used to solve the algebraic system of Eq. (5). The accuracy of this combined numerical technique is not better than that of an usual semi-implicit finite difference discretization in the three dimensions; however, computation times are shorter.

2.3. Model parameters and system specifications

The model contains four model parameters, κ, m, L and ϵ, that are related to the interfacial energy of the grains and the particles and the mobility of the grain boundaries. In order to compare the results of the 3-D simulations with previous 2-D simulations [25], the same parameter values were taken, namely $m = 1$, $\epsilon = 1$, $\kappa = 0.5$, and $L = 1$. Furthermore, the grid spacing Δx and time step Δt were both equal to 1. The particle radius r was taken as equal to 3. However, after discretization, particles were not completely spherical. They had a volume of 88 grid points (g.p.) and a cross-section of 24 g.p. Due to the discretization and the diffuse character of the interfaces, it is in fact difficult to specify accurately the size of these small particles. For most simulations, particles lay in the middle of the film and were randomly distributed throughout the plane of the film. In the discussion, the results of 3-D simulations are compared with those of 2-D simulations for particles with the same size and shape as the cross-section of the 3-D particles. A justification of the parameter choice and particle size is given in Ref. [25].

The simulation systems were $256 \times 256 \times l_3$ or $512 \times 512 \times l_3$ g.p., with l_3 the thickness of the film. l_3 was mostly 15 or 21 g.p. Then the ratio l_3/r is between 5 and 7, which is in the range of the l_3/r-ratios observed for thin Al films with Θ'-$CuAl_2$ particles [7,9]. The simulations were initiated by assigning small random values between -0.001 and 0.001 to all phase field variables at all discrete grid points. Within approximately 50 time steps ($\Delta t = 1$), the random structures evolved towards a fine-grained structure with most of the particles located on a grain boundary (since the particles were present during the nucleation of the grains, the position of the grain boundaries is closely correlated to the position of the particles in this initial structure).

The volume fraction of the second-phase particles f_V in the 3-D simulations is defined as the number of grid points representing the second-phase particles (number of particles × particle volume, i.e. 88 g.p.) divided by the total number of grid points in the system ($l_1 \times l_2 \times l_3$). In the same way, the area fraction of the second-phase particles f_a for 2-D systems is defined as the number of grid points representing the second-phase particles (number of particles × particle area, i.e. 24 g.p.) divided by the total number of grid points in the 2-D system ($l_1 \times l_2$). For the 3-D thin films the area fraction of the particles f_a is defined as the product of the number of particles in the film and the area of the cross-section of the particles (24 g.p.), divided by the area of the film ($l_1 \times l_2$). For columnar grain structures, the radius R of a grain is calculated as $R = \sqrt{A/\pi}$, with A the area of the grain measured in the parallel cross-section through the middle of the film. To visualize the simulation results, the function $\Psi(\vec{r}) = \sum_{i=1}^{p} \eta_i^2(\vec{r})$ is displayed using grey levels, with white representing $\Psi = 1$ and black $\Psi = 0$. Particles appear as black spots, grains are bright and interfaces gray.

3. Comparison between 2-D and 3-D simulations

3.1. Simulation results

In Fig. 1, images of a 3-D simulation are shown. The thickness of the film l_3 was 21 g.p. and the volume fraction of the second-phase particles $f_V = 0.017$ ($f_a = 0.1$). All particles lay in the middle of the film, i.e. the centers of the particles were located in the parallel section through the middle of the film. Only few particles are visible in these 3-D images, since most of the particles are in the bulk of the system. To reveal the grain structure the top and bottom layers of the film are not displayed. They would be dark since the boundary conditions force all phase field variables to become zero at the film surface. Cross-sections through the middle of the film for the same time steps are shown in Fig. 2. At time step 800 (Fig. 1a), the grain structure was approximately columnar. At the beginning of the simulation, grain boundaries passed very easily by the particles. When the grain size increased, the driving force for grain growth decreased and became too low to overcome the pinning pressure of the particles. More and more grain boundaries got pinned by the particles. After about 42,000 time steps, the grain structure was completely pinned. Different from 2-D simulations, the number of grain boundary–particle intersections decreased considerably during grain growth. In the final microstructure, many par-

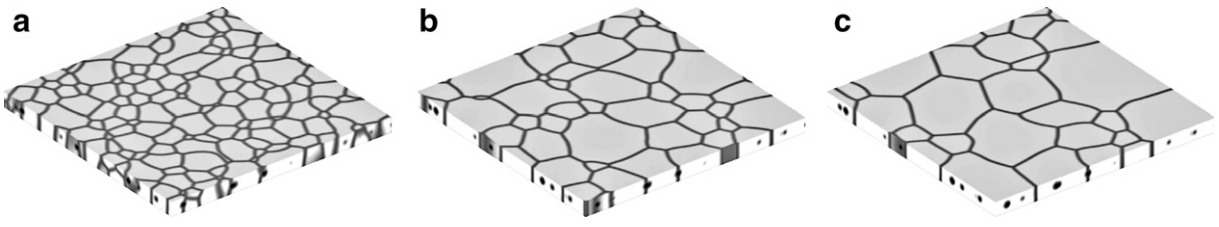

Fig. 1. 3-D simulation images at time steps (a) 800, (b) 6000 and (c) 42,000 of the evolution of the grain structure of a polycrystalline film containing second-phase particles located in the middle of the film for $f_V = 0.017$ and system size $512 \times 512 \times 21$ g.p. ($f_a = 0.1$). $256 \times 256 \times 17$ grid points are shown. The bottom and top layers of the film are not displayed in order to reveal the grain structure. The last structure at time step 42,000 is completely pinned by the particles. Parallel cross-sections through the middle of the film are shown in Fig. 2.

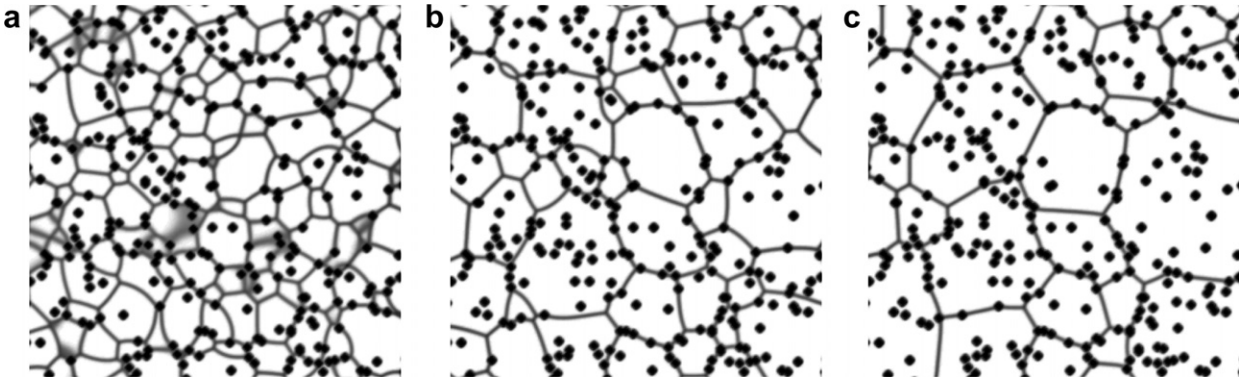

Fig. 2. Parallel cross-sections through the middle of the film for the system depicted in Fig. 1: (a) $t = 800$, (b) $t = 6000$ and (c) $t = 42{,}000$.

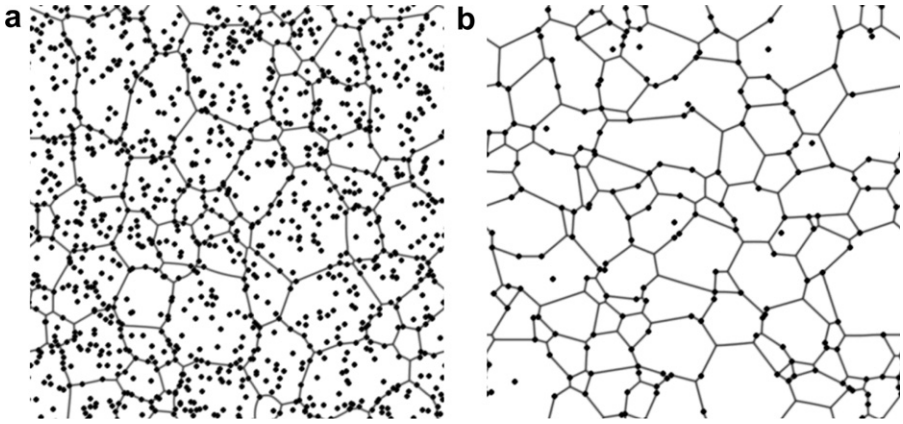

Fig. 3. (a) Cross-section through the middle of the film of a pinned structure obtained from a 3-D simulation for $f_V = 0.017$ and system size $512 \times 512 \times 21$ (the same system as depicted in Figs. 1 and 2). No further evolution was observed after about 42,000 time steps. The final mean grain radius $\overline{R}_{lim}$ is approximately 36 g.p. (b) Pinned microstructure obtained from a 2-D simulation for the same fraction of particles $f_a = 0.017$ and system size 512×512. No further evolution was observed after about 20,000 time steps. The final mean grain radius $\overline{R}_{lim}$ is approximately 30 g.p.

ticles were within the grains. Notice that in the final parallel section in Fig. 2 particles and grain boundary triple junctions are connected by straight lines; hence, in thin films, the grain boundaries have the tendency to become flat.

In Fig. 3, the final parallel section of Fig. 2 is compared with the pinned grain structure obtained in a 2-D simulation for $f_a = 0.017$. The microstructures are very different. In the 2-D system, most particles are in contact with a grain boundary ($\phi \approx 1$), whereas in the 3-D system many particles lie within the grains ($\phi < 1$). Although the fraction of second-phase particles in both systems is equal (the number of particles is even smaller in the 2-D system), the 2-D grain structure is pinned faster than the 3-D columnar structure and its final grain size is smaller. The pinning effect of second-phase particles is obviously much stronger in 2-D systems than in 3-D columnar structures.

3.2. Discussion

Fig. 4 gives a schematic representation of the interaction of a grain boundary with a spherical particle in 3-D and with a circular particle in 2-D.

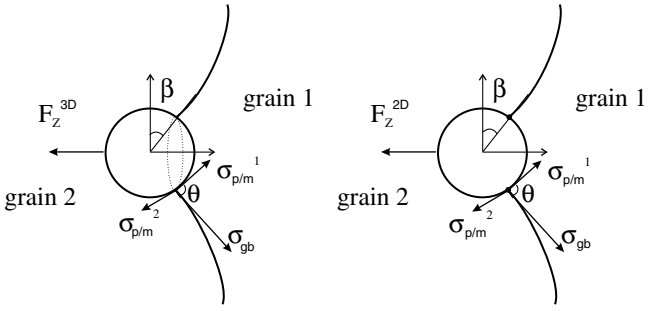

Fig. 4. Schematic representations of a grain boundary pinned by a particle: (a) a spherical particle in 3-D and (b) a circular particle in 2-D. In 3-D the particle–matrix interface and the grain boundary intersect along a circular line with length $2\pi r\cos\beta$, indicated by the dotted line. In 2-D the particle–matrix interface and the grain boundary intersect at two distinct points, indicated by a dot. In both cases, the grain boundary obtains a dimple shape in order to balance the grain boundary tension σ_{gb} and interfacial tensions $\sigma^1_{p/m}$ and $\sigma^2_{p/m}$ of the particle–matrix interface at the intersection line or points. The angle θ depends on $\sigma^1_{p/m}$, $\sigma^2_{p/m}$ and σ_{gb}, and is constant during passage of the grain boundary. The angle β increases while the grain boundary moves from left to right. The grain boundary breaks free from the particle for $\beta = \theta/2$ in 3-D and $\beta = \theta$ in 2-D.

In 3-D, the grain boundary and the particle–matrix interface meet each other along a circular line, which is indicated with a dotted line in Fig. 4a. It can be analytically calculated [10–12] that the force exerted by a spherical particle with radius r on a bypassing grain boundary equals

$$F_Z^{3\text{-D}} = 2\pi r\sigma_{gb}\cos\beta\cos(\theta-\beta) \quad (6)$$

with the angles θ and β as indicated in Fig. 4 and σ_{gb} the specific grain boundary energy or grain boundary tension. The grain boundary obtains a so-called 'dimple' or 'catenoid' shape in order to balance the interfacial tensions $\sigma^1_{p/m}$ and $\sigma^2_{p/m}$ of the particle–matrix interface and the grain boundary tension σ_{gb} in the direction tangential[1] to the particle–matrix interface. The angle θ depends on the interfacial tensions $\sigma^1_{p/m}$, $\sigma^2_{p/m}$ and σ_{gb}, and is constant during passage of the grain boundary. The angle β, at which the grain boundary meets the particle, increases while the grain boundary passes by the particle. The pinning force $F_Z^{3\text{-D}}$ (6) is maximal for $\beta = \beta_{crit}^{3\text{-D}} = \theta/2$. When the maximum pinning force is reached, an instability occurs and the grain boundary breaks free from the particle [12,14,36,44]. Due to the dimple shape, the particle pins the grain boundary over a larger distance than its radius r. In the case of isotropic particle–matrix interfacial tension ($\sigma^1_{p/m} = \sigma^2_{p/m}$), $\theta = \pi/2$ and the grain boundary breaks free from the particle when β is slightly beyond $\beta_{crit}^{3\text{-D}} = \pi/4$.

In 2-D, the grain boundary and the particle–matrix interface only meet in two singular points. The pinning force of the particle is

$$F_Z^{2\text{-D}} = 2\sigma_{gb}\cos(\theta-\beta) \quad (7)$$

The force is maximal when the grain boundary meets the particle at an angle $\beta = \beta_{crit}^{2\text{-D}} = \theta$, instead of $\beta_{crit}^{3\text{-D}} = \theta/2$ in 3-D. Therefore, it is much more difficult for a grain boundary to break free once it is pinned by a particle. Simulations in Ref. [34] also show that it is more difficult for a circular grain in 2-D than for a spherical grain in 3-D to escape from a particle. As a consequence, after a short period of grain growth, most of the particles are located on a grain boundary in 2-D structures.

The consecution of perpendicular sections in Fig. 5 reveals that each time the columnar grain boundaries pass a particle, they temporarily obtain a curvature in the dimension perpendicular to the plane of the film. Hence, the interaction is 3-D. The curvature is required to balance the interfacial tensions at the triple junction where the grain boundary and the particle–matrix interface intersect (indicated with a dotted line in Fig. 4). The extra curvature also contributes to the driving force for grain growth P_g (expressed per unit of grain boundary area) [40,45]

$$P_g = \alpha\sigma_{gb}(K_\parallel + K_\perp) \quad (8)$$

[1] It is assumed that the particle cannot adapt its shape to balance the interfacial tensions perpendicular to the particle–matrix interface.

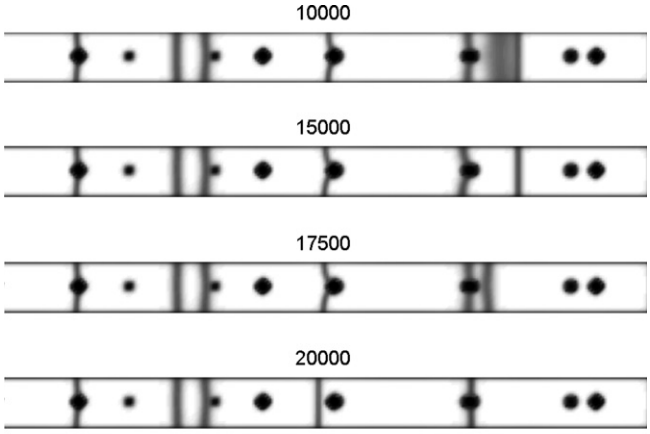

Fig. 5. Perpendicular sections at different time steps of the system depicted in Fig. 1. When a grain boundary meets a particle, it obtains an extra curvature out of the plane of the film. Once the grain boundary has passed the particle, it becomes columnar again.

with α a geometric constant and $K_\parallel$ and $K_\perp$ the local curvatures, respectively, parallel with and perpendicular to the plane of the film.

Although the second-phase particles introduce locally a 3-D effect in the grain boundary migration, the grain structure is still mainly columnar and shows 2-D grain growth behavior. The parallel sections in Fig. 2 show that the columnar grain boundaries easily become straight. This is a typical 2-D feature, since the topological requirements at triple junctions are less complicated in 2-D structures than in 3-D structures [40,45]. Once the grain boundaries are straight, there is no driving force left for grain boundary migration. A columnar grain structure is thus probably more easily pinned than a fully 3-D structure, despite the 3-D character of the grain boundary–particle interaction.

From Fig. 4a, it is also clear that in the case of non-spherical particles the particles are most efficient in pinning columnar grain boundaries when oriented with their largest dimension perpendicular to the plane of the film.

In the above analysis, it is assumed that the grain boundary does not go through the particle [41], that the particle cannot change shape nor rotate [46,47] during passage of the grain boundary and that the grain boundary has its equilibrium shape while passing by the particle. Each of these phenomena may affect the value of the angle θ and retard the escape of the grain boundary (i.e. the grain boundary breaks free at $\beta > \beta_{crit}$). However, the main conclusion remains: in 2-D structures it is more difficult for grain boundaries to escape from particles because $\beta_{crit}^{2\text{-D}} \approx 2\beta_{crit}^{3\text{-D}}$.

4. Film thickness and position of the particles

Fig. 6 presents simulation results for films with different thicknesses. All films contained the same volume fraction of particles, $f_V = 0.024$, and all particles lay in the middle of the film. Accordingly, thicker films contained more

particles (the area fraction of the particles is higher) in order to have the same volume fraction. The data clearly show a transition from a 2-D towards a 3-D particle–grain boundary interaction. The final grain size decreases with film thickness in the 2-D regime and increases with film thickness in the 3-D regime. Furthermore, at the transition from 2-D to 3-D interaction behavior, there is a large decrease in ϕ_{lim} the fraction of particles in contact with a grain boundary in the final microstructure.

In the 2-D regime, the grain boundaries cannot obtain the curvature perpendicular to the film when passing by a particle. Here, the final grain size is in fact a function of the area fraction of the particles and independent of the film thickness. The decrease in final grain size with film thickness in Fig. 6(a) is because there were more particles in the thicker films. ϕ_{lim} slightly decreases with film thickness in the 2-D regime, although one would expect a slight increase, as in 2-D structures ϕ_{lim} increases with the area fraction of the second-phase particles [25]. The small decrease is probably due to the fact that during the very initial time steps (about 100–150 time steps), when the grain boundary structure was not yet columnar, grain boundaries more frequently escaped from particles in the 3-D films than in the 2-D structures.

In the 3-D regime, the fraction of grain boundary–particle intersections decreases and the final grain size increases with film thickness, since in thicker films grain boundaries more easily adapt a curvature out of the plane of the film. Moreover, when films are thicker, more 3-D grain growth – where the pinning effect is smaller – occurs before the grain boundaries become columnar. For the same volume fraction and radius of the particles, the final grain size is larger for thicker films, although they contain more particles per unit of film area. One may expect that the increase in final grain size flattens for larger thicknesses of the film. This was not, however, verified since simulations for thicker films required too much computer power.

In Fig. 6, the transition from 2-D to 3-D pinning behavior is at a film thickness of between 9 and 12 g.p., hence the ratio l_3/r is between 3 and 4. However, for an accurate quantitative analysis of the transition region a finer discretization grid is required. In the present study, the results might be affected by the diffuse character of the interfaces, as the interface of the particles and the film surface overlap for film thicknesses up to 9 g.p. Moreover, when there are only a few grid points between the particle and the film surface, the extra curvature perpendicular to the plane of the film is poorly reproduced and the required equilibrium angles between the grain boundary and the particle–matrix interface and between the grain boundary and the film surface are not always obtained. Therefore the transition from 2-D to 3-D interaction behavior is probably predicted at too high a l_3/r-ratio. This discretization effect reduces for finer grid spacings.

A striking finding from the simulations is that particles in the middle of the film are most efficient in pinning the

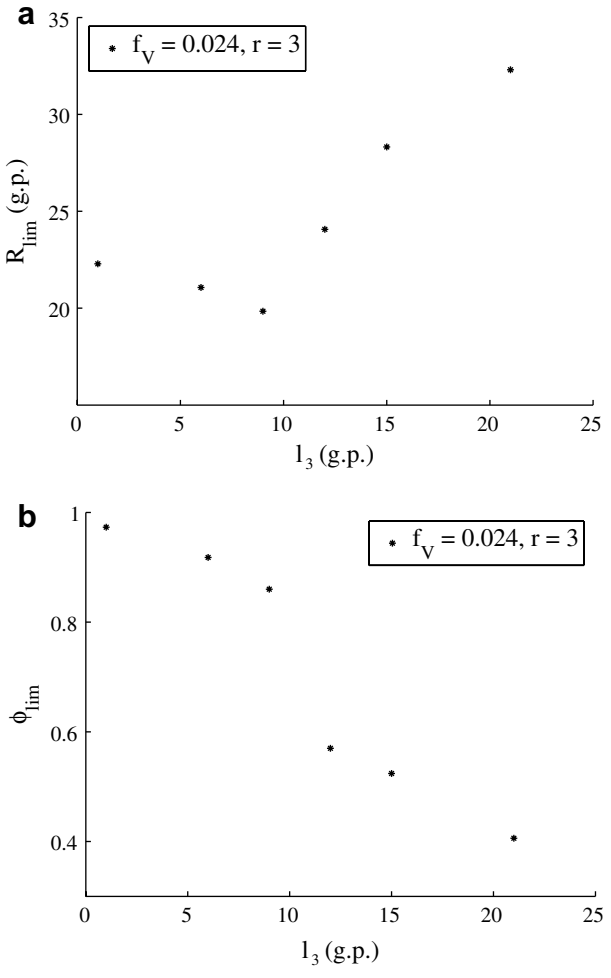

Fig. 6. (a) Final mean grain radius $\overline{R}_{\text{lim}}$ and (b) fraction of particles in contact with a grain boundary in the final microstructure ϕ_{lim}, both as a function of the film thickness l_3. For all the simulations $f_V = 0.024$, $r = 3$ and the particles were in the middle of the film. $l_3 = 1$ refers to a 2-D simulation.

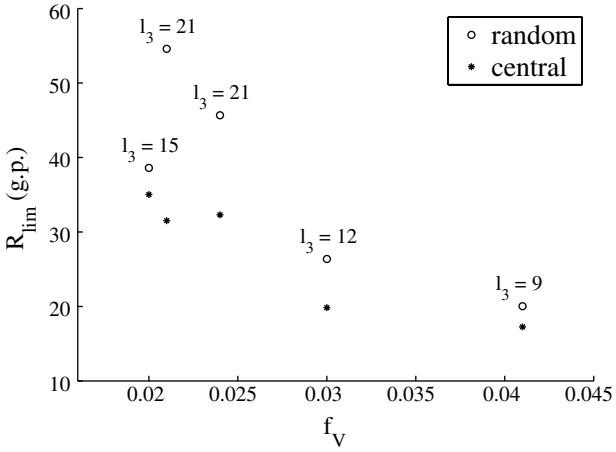

Fig. 7. Comparison of the final mean grain radius $\overline{R}_{\text{lim}}$ for films with all the particles in the middle and films where particles are randomly distributed throughout the thickness of the film.

grain boundaries. Fig. 7 shows that the final mean grain radius $\overline{R}_{lim}$ is consistently smaller for films where all particles are in the middle than for films where particles are randomly dispersed throughout the thickness of the film. The effect of the position of the particles is larger for increasing film thickness and decreasing volume fraction of the particles. It was also observed in experimental studies [7–9], although not understood. A possible explanation is that the columnar structure is more disturbed when particles are located randomly throughout the thickness of the film.

The simulation results in Figs. 6 and 7 show that a relation of the form (1) is too simple for thin films. Besides the volume fraction f_V and the radius r of the particles, the thickness of the film l_3 and the position of the particles throughout the thickness of the film have a major effect on the final grain size of polycrystalline films. For both effects, it is important that the simulation or modelling technique explicitly treats the evolution of the grain boundary shape near grain boundary–particle intersections.

5. Comparison with experimental results

In this section, simulation results from 2-D [25] and 3-D (present work) phase field simulations are compared with experimental data for Al films containing Θ'-$CuAl_2$ precipitates obtained by Longworth and Thompson [9]. The films were produced by electron-beam evaporation of high-purity Al, Cu and Cr on a silicon wafer coated with a SiO_2 film. The initial configuration of the films is schematically shown in Fig. 8a. Thin layers of Cu and Cr were deposited in between two layers of Al with equal thickness. The thickness of the Cu and Cr layers was varied to obtain different volume fractions of the particles. The total thickness of the films was always 0.75 μm. The films were subsequently annealed at around 500 °C for 30 min. The microstructural evolution during annealing was examined using hot-stage transmission electron microscopy.

At the very beginning of the annealing process, the layers of Cu and Cr broke up into small islands and reacted with the aluminum through dissolution into the aluminum and the formation of aluminides (see Fig. 8b). Most precipitates were small semi-coherent Θ'-$CuAl_2$ precipitates. They were primarily formed close to the center of the film.

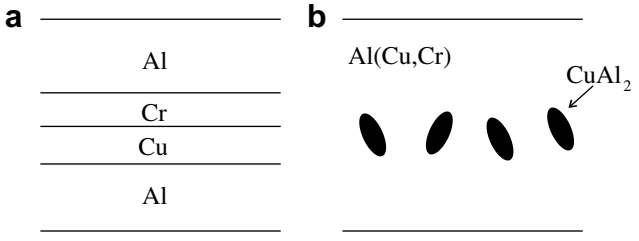

Fig. 8. Schematic representation of the Al films used in the experiments of Longworth and Thompson [9]. The as-deposited configuration, with layers of pure Al, Cu an Cr, is shown on the left. During annealing the layers of Cu and Cr break up and react with the aluminum. The resulting configuration is shown on the right.

The precipitate size was between 0.05 and 0.15 μm. There were also (Cu,Cr)-aluminides, but they were believed to have a minor contribution to the pinning of the grain boundaries because of their small number. No considerable dissolution or coarsening of the Θ'-$CuAl_2$ precipitates was observed during annealing. After the break up of the layers of Cu and Cr, the Al grains became columnar, with their grain boundaries perpendicular to the plane of the film. When normal grain growth was inhibited by the Θ'-$CuAl_2$ precipitates, a few grains with preferential orientation could grow abnormally. In all cases normal grain growth was clearly stopped prior to the start of abnormal grain growth. In the pinned structure, the Θ'-$CuAl_2$ precipitates were located both at grain boundaries and within the grains (see Fig. 9).

The experimental data of Longworth and Thompson are compared with results from phase field simulations in Fig. 10. The experimental data were determined when normal grain growth was stopped and before the start of abnormal grain growth. The results from 2-D simulations are taken from Ref. [25]. These simulations were for different initial grain size $\overline{R}_0$. For the 3-D simulations the ratio l_3/r was taken as equal to 7, which is close to the l_3/r ratios observed for the Al films. The particles were located in the center of the film, as in the investigated Al films. Since grain boundary energy and mobility do not appear in the generalized Zener relation (1), no attempt was made to fit the grain boundary energy and mobility of the simulated systems to those of the experimentally investigated Al films. A difference is that in the simulated systems particles were incoherent and spherical, whereas the Θ'-$CuAl_2$ precipitates were semi-coherent and not fully spherical. The abnormal grain growth after grain growth stagnation was not considered in the simulations.

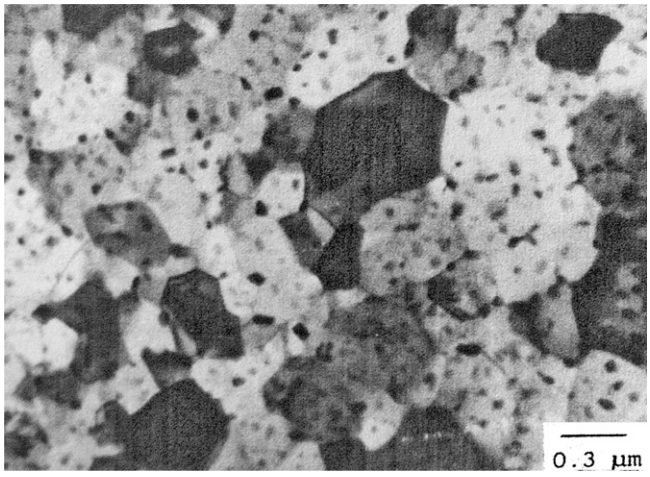

Fig. 9. Hot-stage transmission electron microscopy image of a grain structure pinned by Θ'-$CuAl_2$ precipitates in an Al-alloy film (obtained by Longworth and Thompson [9]). Particles (small dark spots) are located at grain boundaries and in the grains. The larger dark spots are probably unreacted islands of the Cu and Cr layer. The area fraction of the particles is approximately 0.086.

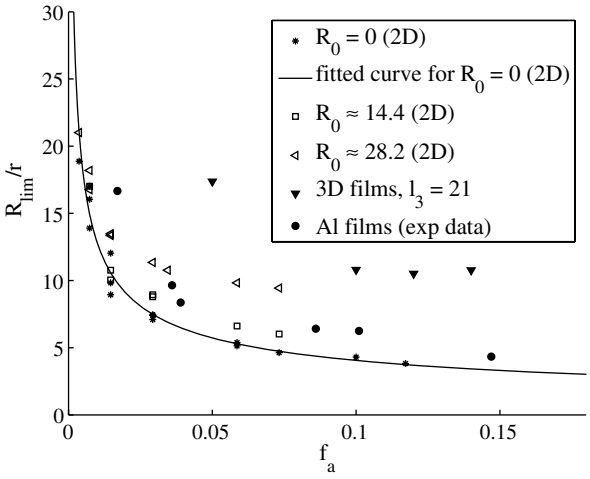

Fig. 10. 2-D and 3-D phase-field simulation results compared with experimental data for Al films containing Θ'-$CuAl_2$ precipitates [9]. 2-D simulations [25] were performed for different initial grain sizes $\overline{R}_0$. $\overline{R}_0 = 0$ corresponds to a random initial structure. The fitted curve follows a generalized Zener relation (1) with $K = 1.28$ and $b = 0.5$. All 3-D simulations (present work) were for $\overline{R}_0 = 0$. (The data point at $f_a = 0.05$ for the 3-D simulated films is only indicative, since there were less than 10 grains in the final microstructure.)

The experimental values for the final mean grain size $\overline{R}_{lim}$ correspond best with the results obtained from 2-D simulations. They follow an approximately $f_a^{-0.5}$ dependence; however, they are systematically above the relation for $\overline{R}_0 = 0$. Since the precipitates were formed at the very beginning of the experiments, prior to considerable grain growth, it is unlikely that this deviation is due to a finite initial grain size (cf. the analysis for $\overline{R}_0 > 0$ in Ref. [25]). Moreover, the deviation is independent of the area fraction of the particles, whereas the effect of initial grain size increases with the area fraction of the particles in 2-D systems [25]. The final grain sizes obtained in the 3-D simulations are much too large, though the microstructures obtained in 3-D simulations with many particles inside the grains (Fig. 11a) are more realistic than those observed in 2-D simulations (Fig. 11b).

Longworth and Thompson compared their experimental data with different analytical theories for Zener pinning. Because of the good correspondence with the analytical relation for 2-D systems of Srolovitz et al. [15], they concluded that the pinning effect of particles is 2-D in thin films. However, the 3-D simulations presented in this article indicate that the agreement with a generalized Zener relation of the form (1) for 2-D systems is rather by coincidence. In the case of thin films, there are many more parameters that influence the final grain size. Surface grooving, for example, results in an extra pinning of the grain boundaries. Furthermore, the Θ'-$CuAl_2$ precipitates were semi-coherent. These effects are not considered in a generalized Zener relation. They were also not considered in the 3-D simulations. Both phenomena result in lower values for $\overline{R}_{lim}/r$. Incorporation of these phenomena into the phase field model would considerably increase its applicability. It would also be interesting to account for orientation dependence of the surface energy of the grains, so that the model can predict the abnormal grain growth observed in the experiments.

6. Conclusions

The pinning effect of second-phase particles on grain growth in polycrystalline films was studied by means of 3-D phase field simulations. A novel methodology that combines the Fourier-spectral method for the dimensions parallel with the film with a finite difference discretization along the dimension perpendicular to the film was proposed to solve the phase field equations for thin films.

Up to now, the pinning effect in thin films was always treated with 2-D analytical models and simulations, resulting in erroneous results. The simulations showed that, although grain growth in thin films is essentially 2-D, the interaction of the columnar grain boundaries with the particles is 3-D. The columnar grain boundaries

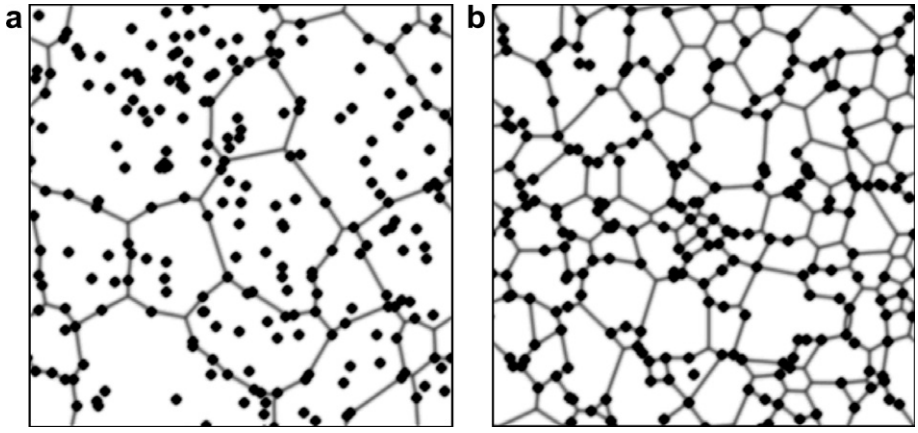

Fig. 11. (a) Image of a pinned structure obtained from a 3-D simulation for $l_3/r = 7$, $f_a = 0.08$ and all particles located in the middle of the film. A planar section through the middle of the film is shown. (b) Image of a pinned microstructure obtained from a 2-D simulation for $f_a = 0.08$ and $\overline{R}_0 = 0$.

temporarily obtain a curvature perpendicular to the plane of the film when passing by a particle. Due to the 3-D character of the pinning interaction, grain boundaries can more easily break free from particles than in 2-D systems. As a consequence, the number of particles in contact with a grain boundary is smaller and the final grain size is larger. The microstructures obtained in 3-D simulations correspond better with experimentally observed microstructures.

The simulations predicted a transition from a 2-D to a 3-D interaction geometry as a function of particle size and film thickness. In the 3-D regime, the final grain size increases and the fraction of particles in contact with a grain boundary decreases with film thickness for a given volume fraction and radius of the particles. Moreover, the simulations revealed that particles in the middle of the film are most efficient in pinning grain boundaries. These findings are omitted in classical Zener type theories or 2-D simulations, although they might be interesting from an application point of view.

Comparison of the simulation results with experimental data for thin Al-alloy films with Θ'-$CuAl_2$ precipitates showed that the properties of the particle–matrix interface and the surface energy of the grains have an import effect on the pinning force of the particles and the final grain size of the films. These effects should be considered in future simulations in order to obtain better quantitative predictions.

The presented model is quite demanding from a computational point of view and, as a consequence, the accuracy of the simulation results was often restricted by limitations in computer power. When more phenomena, like the properties of the particle–matrix interface or anistropy in grain boundary properties, are included, the simulations will require even more computer power. Therefore, it might be interesting to examine the possibilities of other phase field models to treat Zener pinning, for example the vector-valued phase field model of Warren and Kobayashi [48], where only two phase field variables are used to represent all grain orientations in a 3-D system. Another approach would be to develop more specific numerical techniques that exploit the fact that for grain growth simulations the phase field variables equal zero in most grid points.

Acknowledgements

The authors wish to acknowledge the Institute for the Promotion of Innovation through Science and Technology in Flanders (IWT-Vlaanderen) for funding this research. They also thank Prof. C.V. Thompson for providing them with TEM micrographs of his experiments on Al-alloy films.

References

[1] Thompson CV. Annu Rev Mater Sci 1990;20:245.
[2] Thompson CV. Annu Rev Mater Sci 2000;30:159.
[3] Mullins WW. Acta Metall 1958;6:414.
[4] Lou C, Player MA. J Phys D: Appl Phys 2002;35:1805.
[5] Floro JA, Thompson CV. Acta Metall Mater 1993;41:1137.
[6] Thompson CV, Carel R. J Mech Phys Solids 1996;44:657.
[7] Gangulee A, D'Heurle FM. Thin Solid Films 1972;12:399.
[8] Gangulee A, D'Heurle FM. Thin Solid Films 1973;16:227.
[9] Longworth HP, Thompson CV. J Appl Phys 1991;69:3929.
[10] Nes E, Ryum N, Hunderi O. Acta Metall 1985;33:11.
[11] Manohar PA, Ferry M, Chandra T. ISIJ Int 1998;38:913.
[12] Ashby MF, Harper J, Lewis J. Trans Metall Soc AIME 1969;245:413.
[13] Hellman P, Hillert M. Scand J Met 1975;4:211.
[14] Wörner C, Cabo A, Hillert M. Scripta Metall 1986;20:829.
[15] Srolovitz DJ, Anderson MP, Grest GS, Sahni PS. Acta Metall 1984;32:1429.
[16] Anderson MP, Grest GS, Doherty RD, Li K, Srolovitz DJ. Scr Metall 1989;23:753.
[17] Gao J, Thompson RG, Patterson BR. Acta Mater 1997;45:3653.
[18] Soucail M, Messina R, Cosnuau A, Kubin LP. Mater Sci Eng A 1999;271:1.
[19] Miodownik M, Holm EA, Hassold GN. Scripta Mater 2000;42:1173.
[20] Riege SP, Thompson CV, Frost HJ. Acta Mater 1999;47:1879.
[21] Weygand D, Bréchet Y, Lépinoux J. Acta Mater 1999;47:961.
[22] Weygand D, Bréchet Y, Lépinoux J. Mater Sci Eng A – Struct Mater Prop Microstruct Process 2000;292:34.
[23] Fan D, Chen L-Q, Chen S-PP. J Am Ceram Soc 1998;81:526.
[24] Steinbach I, Apel M. Advances in materials theory and modeling - bridging over multiple-length and time scales. In: Materials research society symposium proceedings, vol. 677, April 16–20, 2001, San Francisco, p. AA7.14.1.
[25] Moelans N, Blanpain B, Wollants P. Acta Mater 2006;54:1175.
[26] Suwa Y, Saito Y, Onodera H. Scripta Mater 2006;55:407.
[27] Couturier G, Doherty R, Maurice C, Fortunier R. Acta Mater 2005;53:977.
[28] Frost HJ, Thompson CV. J Electron Mater 1988;17:447.
[29] Fayad W, Thompson CV, Frost HJ. Scripta Mater 1999;40:1199.
[30] Frost HJ, Thompson CV, Walton DT. Acta Metall Mater 1990;38:1455.
[31] Frost HJ, Thompson CV, Walton DT. Acta Metall 1992;40:779.
[32] Carel R, Thompson CV, Frost HJ. Acta Mater 1996;44:2479.
[33] Ko YK, Jang JH, Lee S, Yang HJ, Lee WH, Lee JG. J Mater Sci: Mater Electron 2003;14:103.
[34] Moelans N, Blanpain B, Wollants P. Acta Mater 2005;53:1771.
[35] Louat N. Acta Metall 1982;30:1291.
[36] Miodownik M, Martin JW, Cerezo A. Phil Mag A 1999;79:203.
[37] Miodownik M. Scripta Mater 2006;54:993.
[38] Chen L-Q. Scripta Metall Mater 1995;32:115.
[39] Fan D, Chen L-Q. Acta Mater 1997;45:611.
[40] Humphreys FJ, Hatherly M. Recrystallization and related annealing phenomena. Oxford: Pergamon; 1996.
[41] Doherty R. Metal Sci 1982;16:1.
[42] Kril CE, Chen L-Q. Acta Mater 2002;50:3057.
[43] Chen L-Q, Shen J. Comp Phys Commun 1998;108:147.
[44] Ringer S, Kuziak R, Easterling K. Mater Sci Technol 1991;7:193.
[45] Atkinson HV. Acta Metall 1988;36:469.
[46] Ringer SP, Li WB, Easterling KE. Acta Metall 1989;37:831.
[47] Ringer S, Li W, Easterling K. Acta Metall Mater 1992;40:275.
[48] Warren JA, Kobayashi R, Lobkovsky E, Carter WC. Acta Mater 2003;51:6035.